

## ARTICLE OPEN

## Understanding the reactivity of CoCrMo-implant wear particles

Mohamed A. Koronfel<sup>1</sup>, Angela E. Goode<sup>1</sup>, Johanna Nelson Weker<sup>2</sup>, Stephen E. R. Tay<sup>1</sup>, Camilla A. Stitt<sup>1</sup>, Thiago A. Simoes<sup>3</sup>, J. Frederick W. Mosselmans<sup>4</sup>, Paul Quinn<sup>4</sup>, Rik Brydson<sup>3</sup>, Alister Hart<sup>5</sup>, Michael F. Toney<sup>2</sup>, Alexandra E. Porter<sup>1</sup> and Mary P. Ryan<sup>1</sup>

CoCrMo-based metal-on-metal hip implants experienced unexpectedly high failure rates despite the high wear and corrosion resistance of the bulk material. Although they exhibit a lower volumetric wear compared to other implant materials, CoCrMo-based implants produced a significantly larger 'number' of smaller wear particles. CoCrMo is nominally an extremely stable material with high Cr content providing passivity. However, despite the Co:Cr ratio in the original alloy being 2:1; chemical analyses of wear particles from periprosthetic tissue have found the particles to be composed predominately of Cr species, with only trace amounts of Co remaining. Here a correlative spectroscopy and microscopy approach has shown that these particles dissolve via a non-stoichiometric, and geometrically inhomogeneous, mechanism similar to de-alloying. This mechanism is previously unreported for this material and was not apparent in any of the regulatory required tests, suggesting that such tests are insufficiently discriminating.

*npj Materials Degradation* (2018)2:8; doi:10.1038/s41529-018-0029-2

## INTRODUCTION

CoCrMo alloys have been used as a biomaterial for metal-on-metal (MOM) hip implants because of their high corrosion resistance and significantly lower volumetric wear compared to metal-on-polyethylene (MOP) implants.<sup>1</sup> This made them less likely to fail due to osteolysis (bone resorption due to an inflammatory response<sup>2,3</sup> induced mainly by polyethylene and Ti particles and leading to the aseptic loosening of the implant), the most common hip implant failure mechanism.<sup>4</sup> However, CoCrMo-based hip implants suffered an unexpectedly high failure rate, with many patients experiencing unexplained pain, leading to revision surgery. Simulation studies have since revealed that, despite the lower 'volumetric' wear, CoCrMo alloys produce a much higher number of smaller wear particles: up to 'one trillion' nanoscale particles per patient annually.<sup>5</sup> These wear particles trigger an inflammatory immune response thought to be linked to implant failure,<sup>6</sup> although the mechanistic details remain poorly understood.

Studies on periprosthetic tissue from failed implants have shown that CoCrMo wear particles are found inside macrophage cells.<sup>1,7,8</sup> Widespread dissemination of metal wear debris has also been established in post-mortem studies with particles found within macrophages and extracellularly in the synovial membrane, lymph nodes and bone marrow,<sup>9</sup> in addition to accumulating in macrophage cells in the liver and spleen.<sup>10</sup> A number of studies have characterised the chemical composition of particles from periprosthetic tissue, in order to understand the state of wear debris in vivo. Huber et al.<sup>11</sup> examined tissue from 11 cases where inflammatory reactions characteristic of immune response was evident in all. Using scanning electron microscopy–energy dispersive X-ray (SEM-EDX) and Fourier transform infrared (FTIR)

spectroscopies they reported Cr phosphate-like corrosion products, as well as un-corroded metallic particles. However, Catelas et al.<sup>12</sup>, using EDX in the transmission electron microscope (TEM), reported Cr oxide corrosion products among the metallic particles. Addressing this difference in the reported Cr species, Hart et al.<sup>13</sup> used microfocus X-ray absorption spectroscopy to provide additional speciation information complementing the data on elemental composition provided by EDX. They reported the most abundant species to be Cr-phosphate residues. Most recently, Goode et al.<sup>8</sup> used scanning transmission X-ray microscopy- X-ray absorption spectroscopy (STXM-XAS) and scanning transmission electron microscopy- electron energy-loss spectroscopy (STEM-EELS) combining chemical analysis at both high energy and spatial resolution. Their results confirmed the presence of debris in two phases, a minority metallic phase (often found as the 'core' of reacted particle) and a more abundant Cr(III) phase with only trace amounts of oxidised Co. The reported deficiency of Co in wear particles would indicate rapid dissolution of Co, likely into aqueous Co(II), which could then reach the blood stream and be transported away.

Co dissolution raises questions from two different perspectives: clinical and material science. Clinically, it is known that Co(II) ions are cytotoxic and genotoxic,<sup>14,15</sup> but a second major clinical concern which remains unresolved is the mechanism of in vivo dissolution of CoCrMo, a nominally stable material, and the speciation of Cr during this process. Cr(VI) species are known to be carcinogenic; Gill et al. provide a comprehensive review on the clinical risks posed by Co and Cr from implant wear.<sup>16</sup> Furthermore, whilst much attention has been given to the release of Co and Cr ions, recently Simoes et al.<sup>17</sup> found, in the presence of bovine serum albumin (BSA), a much higher release of Mo ions relative to Co and Cr, using inductively

<sup>1</sup>Department of Materials, Imperial College London, London, UK; <sup>2</sup>Stanford Synchrotron Radiation Lightsource, SLAC National Accelerator Laboratory, Menlo Park, USA; <sup>3</sup>School of Chemical and Process Engineering, University of Leeds, Leeds, UK; <sup>4</sup>Diamond Light Source, Didcot, UK and <sup>5</sup>Institute of Orthopaedics and Musculoskeletal Science, Royal National Orthopaedic Hospital, London, UK

Correspondence: Mary P. Ryan (m.p.ryan@imperial.ac.uk)

Received: 26 November 2017 Revised: 04 January 2018 Accepted: 18 January 2018

Published online: 12 March 2018

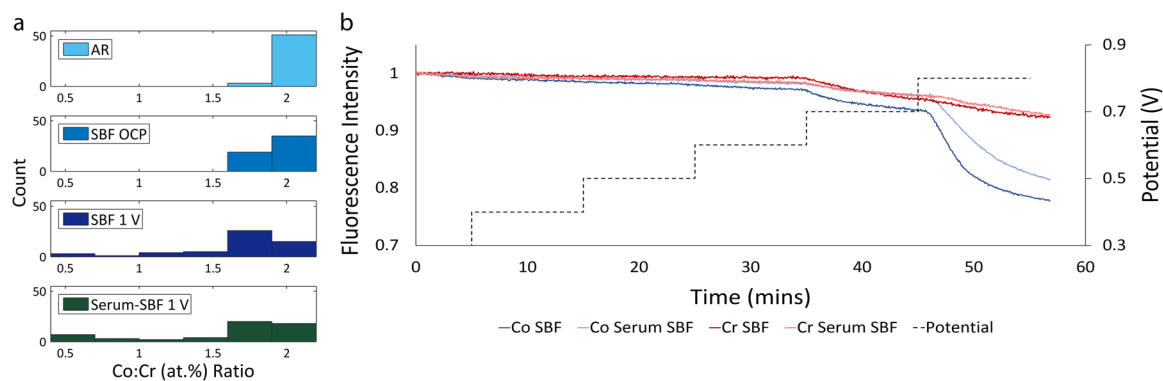


**Fig. 1** **a** Histograms of Co:Cr atomic ratios calculated from EDX analysis of CoCrMo particles in four conditions: As Received (AR), after exposure to SBF at OCP, after exposure to SBF at 1V polarisation, and after exposure to serum-containing SBF at 1V polarisation (54 particles in each condition). **b** Fluorescence intensity of Co (at 7757 eV) and Cr (at 6009 eV) over time. The particles were held at OCP for the first five minutes before the potential was stepped from 0.4 to 0.8 V. A greater drop in the amount of Co compared to Cr is observed after the 0.7 V and 0.8 V steps

coupled plasma mass spectrometry (ICP-MS). The dissolved Mo ions were thought to form complexes with proteins, thus potentially inhibiting their function.

From the material science perspective, the reactivity and release of ionic species from CoCrMo alloys is unexpected. Electrochemically, the oxidation of Co to Co(II) is restricted by passivation in CoCr alloys, which exhibit a strong 'Cr-like' passive behaviour primarily due to the formation of a Cr oxide-based passive film. This passive layer is stable until high potential regions where transpassive release of the Cr(VI) ions occurs ( $\sim 0.5$  V vs SCE in 0.14 M NaCl solution).<sup>18</sup> Therefore, for continued dissolution of Co, the *in vivo* conditions must either allow for transpassive corrosion, or there must be a different dissolution mechanism operating for CoCrMo 'particles'. If Cr(VI) ions were released *in vivo*, they may not be observed *ex situ* due to their transient nature. On the other hand, it is possible that the particles' electrochemical behaviour is different from that of the bulk and Co dissolution occurs before, or without, the release of Cr(VI). High-resolution particle analysis, as well as *in situ* studies are therefore essential to confirm the behaviour of CoCrMo particles during dissolution.

Understanding the failure mechanism of MOM implants is vital in order to identify the clinical risks faced by the tens of thousands of patients who currently have such an implant.<sup>19</sup> In addition, the findings will be essential for building new design, testing and regulatory criteria for future biomedical implants before they attain regulatory approval.

In this work *ex situ* and *in situ* electrochemical experiments were conducted in order to understand the behaviour of CoCrMo wear particles in a simulated macrophage environment. The effect of both bovine serum albumin and an applied electric potential on this behaviour was examined. Such electrochemical experiments have been utilised for accelerated corrosion testing of bulk alloys used in hip implants.<sup>20</sup> In particular it is known that a key part of the immune inflammatory response is the generation of a local oxidising environment (occurring via the production of oxygen and hydroxyl radicals from activated macrophages), which in turn leads to accelerated corrosion.<sup>21</sup> Therefore, by controlling the potential independently, the *in vivo* environment could be mimicked. The studies involved potential scans to determine the onset of dissolution. In selected cases, a single high potential was used as an accelerated test to provide insight on later-stage dissolution.

## RESULTS

A complementary spectroscopy and microscopy approach was used to develop an understanding of the dissolution of the particles based on chemical and morphological changes.

### Ex situ spectroscopy

Firstly, to understand how Co:Cr ratio (at.%) varied as a function of simulated environment, CoCrMo particles were analysed by *ex situ* spectroscopy using TEM-EDX. The conditions were: (i) as-received (AR); or 10 min immersion in either (ii) simulated body fluid (SBF) at open circuit potential (OCP); (iii) SBF while being polarised at 1V; and (iv) serum-SBF while being polarised at 1V. The histograms in Fig. 1a show the variation in Co:Cr atomic elemental ratio, across 54 particles, with each exposure condition. AR particles were composed of Co:Cr in ratios between 1.6 and 2.2. Samples exposed to SBF, at OCP, displayed similar compositions, though a higher percentage of SBF OCP particles with ratios between 1.6–1.9 suggests the onset of limited cobalt dissolution. In clear contrast, Co:Cr ratios of both polarised samples were spread over a large number of lower ratio bins (down to 0.4–0.7), demonstrating a greater loss of Co compared to Cr.

### In situ spectroscopy

To study the dynamics of Co and Cr dissolution from particles, *in situ* X-ray absorption spectroscopy (XAS) experiments were conducted at Beamline I20, Diamond Lightsource, UK. XAS was used to directly monitor the Co and Cr elemental content of a layer of wear particles on a gold working electrode surface. The experiments were done in fluorescence geometry where the measurements were sensitive to the wear particles and not the SBF solution. Single energy time scans were recorded above both the Co and Cr edges. Fig. 1b shows X-ray absorption data for both Co and Cr as a function of time and potential, in SBF and serum-SBF. Each plot represents the average of three independent repeats. Changes in fluorescence intensity can be noticed at the 0.6V step but a clear drop in the intensity (and hence the amount of each element 'remaining' in the particles) was observed for both Co and Cr at the 0.7 V and 0.8 V steps. Furthermore, the fractional change in the amount of Co was larger compared to Cr, revealing a non-stoichiometric dissolution. In SBF, the amount of Co remaining was noticeably lower than Cr after both 0.7V and 0.8V steps (see bar chart in ESI). In serum-SBF, the amount of Co remaining was also noticeably lower than Cr after the 0.8V step.

XANES spectra acquired before and after potential application were similar revealing no significant changes in speciation (see ESI Fig. 1). This validates the use of a single-energy scan to monitor the dissolution of Co and Cr from particles. However, it is noted that speciation of wear particles in periprosthetic tissue showed solid Cr(III) deposits, while these results show no significant change in the oxidation state of Cr. We hypothesise that this is a kinetic effect and the residual Cr observed would have

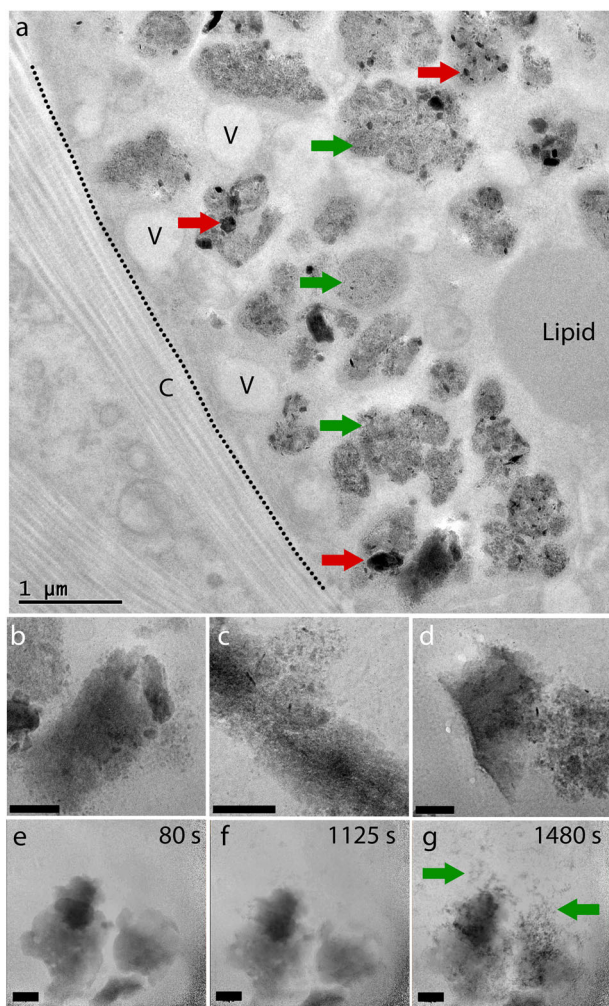


**Fig. 2** **a** TEM image of a macrophage cell from periprosthetic tissue recovered from a patient showing CoCrMo wear debris marked by the red (solid particles) and green (diffuse, less electron dense material) arrows. (Legend: C = collagen, V = vesicles, dotted line = plasma membrane). **b–d** Higher magnification TEM images of CoCrMo wear debris from within the cell in **(a)**, Scale bars = 200 nm. **e–g** A series of in situ TXM images of CoCrMo particle in Agar-SBF recorded during potential scan, revealing the onset of release of diffuse material, Scale bars = 3 μm

transformed to Cr(III) species in the continued oxidising environment of the lysosome.

#### In situ microscopy

The results presented above describe population-averaged measurements. To further elucidate dissolution mechanisms, these results were complemented with studies of morphological changes in single CoCrMo particles. In situ transmission X-ray microscopy (TXM) was performed at Beamline 6–2, Stanford Synchrotron Radiation Lightsources (SSRL, USA). The TXM images shown in Fig. 2e–g (see ESI video 1) have a spatial resolution of 30 nm and a time resolution of 3 s. An X-ray energy of 7810 eV was used to provide contrast at the Co edge. No morphological changes were observed at low potentials, however at 0.56 V, changes in the particle shape can be noted, along with the rapid egress of dissolving material. To our knowledge, this is the first time a TXM-based approach has been used to follow local dissolution behaviour. This sudden onset of morphological change is consistent with the onset of dissolution detected during in situ

spectroscopy, but provides further insights into the nature of the process. The observed “diffuse material” in these TXM images is analogous to the morphology of wear debris observed by TEM in macrophage cells from periprosthetic tissue (Fig. 2a–d).

#### Ex situ microscopy

To obtain further insights into the morphological changes of particles under oxidising conditions, spatially-resolved studies of the morphological changes in single CoCrMo particles were done ex situ using scanning and transmission electron microscopy (SEM and TEM). CoCrMo particles drop-cast on to gold-coated glass slides were polarised at 0.8 V in SBF and serum-SBF. Fig. 3 shows SEM micrographs comparing an AR and SBF particles (both at OCP and also polarised). The development of a porous surface on the polarised SBF particle can be observed in Fig. 3c. This porous surface is not as obviously visible in particles polarised in serum-SBF (Fig. 3d) possibly due to masking of surface topography by the presence of strongly surface-adsorbed proteins.<sup>22</sup>

STEM tomography was used to reveal the sub-surface morphology of particles polarised at 1 V on a TEM grid. Fig. 3e shows a dark field STEM image of the particle after polarisation. Cross-sections through the 3D reconstruction reveal that the porosity was not only present at the surface but also extended through the entire depth of the particle (see ESI video 2).

#### DISCUSSION

The drop of Co:Cr (at. %) ratio, observed by TEM-EDX, reveal the preferential dissolution of Co from the alloy. However, a drop in the Co:Cr ratio only indicates the relative dissolution of the elements, while in this work the absolute loss of Co and Cr was also directly measured independently using in situ XAS. The non-stoichiometric dissolution behaviour was particularly prominent at/above 0.7 V polarisation. Additionally, the XAS results present the Co:Cr drop averaged over a much larger population of particles (thousands compared to only 54 particles measured by TEM-EDX). They showed an approximately 22% drop in Co compared to 6% drop in Cr at the end of the 0.8 V step in SBF. This corresponds to Co:Cr ratio drop from 2 to 1.66. Although 0.7 V is in the transpassive domain for this alloy, the kinetics for Cr dissolution are slower than for Co at this potential; since there is a large effective overpotential for  $\text{Co}^{2+}$  dissolution. Hence the alloy dissolves non-stoichiometrically. The presence of serum appeared to ‘decrease’ the amount of dissolution of Co (and to a much lesser extent, Cr) possibly due to the stabilising effects of protein adsorption on the surface.<sup>22</sup> However, we note that this is in contrast to Mo where the presence of serum has been found to enhance dissolution.<sup>17</sup>

The evolution of the nanoporous structure is characteristic of a dealloying-like process. Dealloying is the dissolution of the more active metal (in this case Co), leading to the aggregation of the noble component (Cr) into clusters by a process similar to phase separation.<sup>23,24</sup> Hence, instead of a uniform protection of the surface, aggregation of Cr atoms only passivates the surface locally. The process of dealloying is consistent with the higher rate of Co loss compared to Cr observed in this work and in vivo. Whilst this finding suggests that ongoing Co dissolution alone is not ‘necessarily’ indicative of Cr(VI) formation, we note that the onset of dissolution may require some local Cr dissolution, and so is facilitated by the onset of transpassivity.

In conclusion, this work represents a correlative approach between microscopy and spectroscopy together with a combination of ex situ and in situ studies: this multimodal approach has provided new insights into the dissolution behaviour of CoCrMo particles. The data consistently show a significantly higher rate of dissolution of Co than Cr in oxidising conditions used here to mimic inflammatory response in vivo. Furthermore, in situ TXM

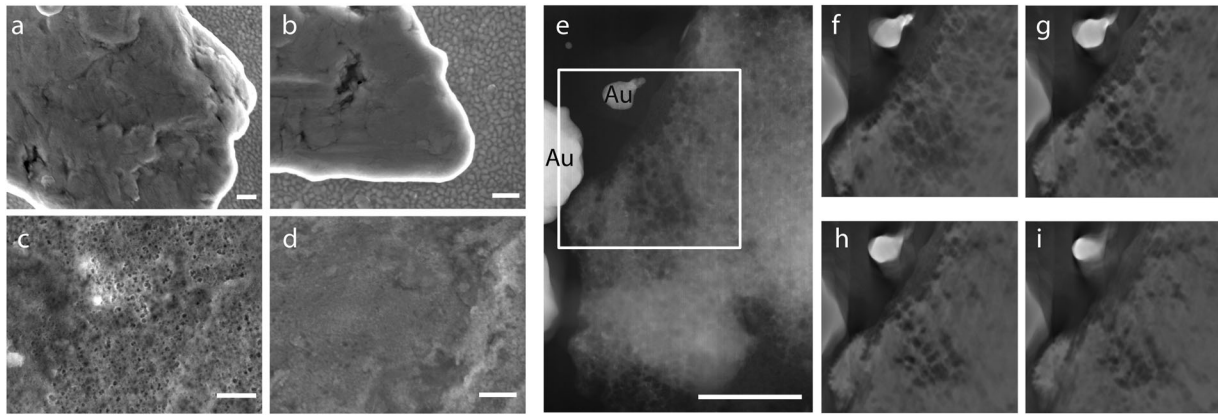


**Fig. 3** Secondary electrons SEM images of (a) AR particle, (b) a particle after exposure to SBF at OCP, (c) a particle after exposure to SBF at 0.8V showing the development of a nano-porous surface, (d) a particle after exposure to serum-SBF at 0.8V. e Dark field STEM image of CoCrMo particle (biased in SBF at 1V), f–i Cross-sections through tomographic reconstructions, 8 nm apart, taken from a  $370 \times 360 \times 40$  nm section outlined by white box in (e). Gold particles (labelled Au) were formed from the TEM grid during polarisation. Scale bars = 200 nm

shows clear evidence of a rapid and inhomogeneous dissolution process, leading to the porous sponge-like structure observed via electron tomography. Taken together these data suggest that the particles undergo a dealloying-like process which was not evident in studies required for the clinical approval of materials. This approach provides valuable evidence on the likely behaviour of particles in vivo and suggests that current methods for material assessment and approval are insufficiently discriminating.

## METHODS

CoCrMo particles were produced by mechanical milling of the bulk standard alloy used in orthopaedic implants ASTM F75 (Co 60, Cr 30, Mo 7%). The particles were fully characterised and have been described in detail by Simoes et al.<sup>25</sup> Depending on the experiment, the particles were drop-cast on to one of: carbon-coated gold TEM grids, gold-coated Kapton films or gold-coated glass slides, which acted as the working electrode. A platinum wire (Sigma-Aldrich, UK) was used as the counter electrode with an Ag/AgCl reference microelectrode, +199 mV vs SHE, (Microelectrodes Inc, USA, against which all potentials are quoted). Simulated body fluid (SBF) at pH 5.2 was used to represent the lysosome environment in a macrophage cell, (25 mM MES buffer, 0.5 mM  $\text{CaCl}_2 \cdot 2\text{H}_2\text{O}$ , 1 mM  $\text{MgCl}_2$ , and 200 mM KCl). In some experiments, to examine the effect of protein, 1  $\mu\text{g}/\text{ml}$  of bovine serum albumin was added to the SBF (serum-SBF). In all experiments the SBF was maintained at 37 °C.

## In situ spectroscopy at diamond beamline I20

Based on a design by Kerkar et al.,<sup>26</sup> particles on gold-coated Kapton film were attached to custom-made electrochemical cell such that the substrate working electrode became the X-ray window in the cell. The beam size was  $400 \times 300 \mu\text{m}^2$  covering a population of ca.2000 particles. The cell was mounted 45° to the incident beam and data collected in reflection geometry. In this arrangement the intensity of the fluorescence signal is directly proportional to the amount of material remaining in substrate-bound particles; this presents a very sensitive method to measure in situ the dissolution process, as species which rapidly diffuse away from the X-ray window do not contribute to the signal. Fluorescence intensity was monitored over time, at photon energies of 6009 and 7757 eV for Cr and Co respectively, as the potential was stepped from 0.4 to 0.8 V. Full XANES spectra were collected at the beginning and end of the in situ experiments.

## In situ microscopy at SSRL beamline 6-2

CoCrMo particles were imaged in situ using a 3D printed electrochemical cell (details previously reported in ref. 27). To capture the onset of morphological changes, TXM images were collected as the potential was scanned from 0 to 0.7 V (at 0.5 mV/s). Agarose was added to the SBF in this experiment to increase the electrolyte viscosity and hence the chance of capturing diffusing material (away from surface).

## Data availability

The data that support the findings of this study are available from the corresponding author upon reasonable request.

## ACKNOWLEDGEMENTS

M.A.K. was supported by the EPSRC Centre for Doctoral Training in Advanced Characterisation of Materials (grant number EP/L015277/1). M.P.R. acknowledges funding from the Royal Academy of Engineering and Shell Global Solutions via the Research Chair Scheme. We thank Diamond Light Source for access to beamline I20 (SP4843, SP9797) that contributed to the results presented here. Use of the Stanford Synchrotron Radiation Lightsource, SLAC National Accelerator Laboratory, is supported by the U.S. Department of Energy, Office of Science, Office of Basic Energy Sciences under Contract No. DE-AC02-76SF00515.

## AUTHOR CONTRIBUTIONS

The work described in this paper forms part of M.A.K.'s PhD thesis; all experiments were carried out by M.A.K. and A.E.G. The project was conceived and designed by M. P.R., A.E.P. and A.E.G. who also supervised M. A. K. during the project. Simulated wear particles were prepared and characterised by T.S. and R.B.A.H. provided clinical insights and access to biological samples. J.N.-W. and M.F.T. co-designed the TXM (SSRL) experiments and contributed to TXM data analysis; S. E. R. T. contributed to TXM experimental-cell design and data collection. J.F.W.M., P.Q. and C.A.S. assisted in the XAS experiments and analysis (Diamond). All authors contributed to interpretation of the data and preparation of the manuscript.

## ADDITIONAL INFORMATION

**Supplementary information** accompanies the paper on the *npj Materials Degradation* website (<https://doi.org/10.1038/s41529-018-0029-2>).

**Competing interests:** A.H. had research contracts with nine orthopaedic manufacturers regarding metal on metal hip implants: Zimmer, Stryker, Depuy, Corin, Biomet, JRI, Mathys, Finsbury, Smith and Nephew. All other authors declare no competing financial interests.

**Publisher's note:** Springer Nature remains neutral with regard to jurisdictional claims in published maps and institutional affiliations.

## REFERENCES

1. Doorn, P. F. et al. Metal wear particle characterization from metal-on-metal total hip replacements: transmission electron microscopy study of periprosthetic tissues and isolated particles. *J. Biomed. Mater. Res.* **42**, 103–111 (1998).
2. Ingham, E. & Fisher, J. The role of macrophages in osteolysis of total joint replacement. *Biomaterials* **26**, 1271–1286 (2005).
3. Veronesi, F., Tschon, M. & Fini, M. Gene expression in osteolysis: review on the identification of altered molecular pathways in preclinical and clinical studies. *Int. J. Mol. Sci.* **18**, 499 (2017).

4. Ulrich, S. D. et al. Total hip arthroplasties: What are the reasons for revision? *Int. Orthop.* **32**, 597–604 (2008).
5. Catelas, I. et al. Size, shape, and composition of wear particles from metal-metal hip simulator testing: effects of alloy and number of loading cycles. *J. Biomed. Mater. Res. A* **67**, 312–327 (2003).
6. Konttinen, Y. T. & Pajarinen, J. Surgery: Adverse reactions to metal-on-metal implants. *Nat. Rev. Rheumatol.* **9**, 5–6 (2013).
7. Delaunay, C., Petit, I., Learmonth, I. D., Oger, P. & Vendittoli, P. A. Metal-on-metal bearings total hip arthroplasty: The cobalt and chromium ions release concern. *Orthop. Traumatol. Surg. Res.* **96**, 894–904 (2010).
8. Goode, A. E. et al. Chemical speciation of nanoparticles surrounding metal-on-metal hips. *Chem. Commun.* **48**, 8335 (2012).
9. Case, C. P. et al. Widespread dissemination of metal debris from implants. *J. Bone Jt. Surg. Br.* **76**, 701–712 (1994).
10. Urban, R. M., Tomlinson, M. J., Hall, D. J. & Jacobs, J. J. Accumulation in liver and spleen of metal particles generated at nonbearing surfaces in hip arthroplasty. *J. Arthroplast.* **19**, 94–101 (2004).
11. Huber, M., Reinisch, G., Trettenhahn, G., Zweymüller, K. & Lintner, F. Presence of corrosion products and hypersensitivity-associated reactions in periprosthetic tissue after aseptic loosening of total hip replacements with metal bearing surfaces. *Acta Biomater.* **5**, 172–180 (2009).
12. Catelas, I., Campbell, P. A., Bobyn, J. D., Medley, J. B. & Huk, O. L. Wear particles from metal-on-metal total hip replacements: effects of implant design and implantation time. *Proc. Inst. Mech. Eng. Part H. J. Eng. Med.* **220**, 195–208 (2006).
13. Hart, A. J. et al. Microfocus study of metal distribution and speciation in tissue extracted from revised metal on metal hip implants. *J. Phys. Conf. Ser.* **190**, 12208 (2009).
14. Kwon, Y.-M. et al. Dose-dependent cytotoxicity of clinically relevant cobalt nanoparticles and ions on macrophages in vitro. *Biomed. Mater.* **4**, 25018 (2009).
15. Papageorgiou, I. et al. Genotoxic effects of particles of surgical cobalt chrome alloy on human cells of different age in vitro. *Mutat. Res. - Fundam. Mol. Mech. Mutagen.* **619**, 45–58 (2007).
16. Gill, H. S., Grammatopoulos, G., Adshead, S., Tsialogiannis, E. & Tsiridis, E. Molecular and immune toxicity of CoCr nanoparticles in MoM hip arthroplasty. *Trends Mol. Med.* **18**, 145–155 (2012).
17. Simoes, T. A. et al. Evidence for the dissolution of molybdenum during tribo-corrosion of CoCrMo hip implants in the presence of serum protein. *Acta Biomater.* **45**, 410–418 (2016).
18. Hodgson, A. W. E. et al. Passive and transpassive behaviour of CoCrMo in simulated biological solutions. *Electrochim. Acta* **49**, 2167–2178 (2004).
19. Bozic, K. J. et al. The Epidemiology of Revision Total Hip Arthroplasty in the United States. *J. Bone Jt. Surg.* **91**, 128–133 (2009).
20. Khan, M. A., Williams, R. L. & Williams, D. F. In-vitro corrosion and wear of titanium alloys in the biological environment. *Biomaterials* **17**, 2117–2126 (1996).
21. Mabileau, G. et al. Influence of fluoride, hydrogen peroxide and lactic acid on the corrosion resistance of commercially pure titanium. *Acta Biomater.* **2**, 121–129 (2006).
22. Valero Vidal, C. & Igual Muñoz, A. Electrochemical characterisation of biomedical alloys for surgical implants in simulated body fluids. *Corros. Sci.* **50**, 1954–1961 (2008).
23. Erlebacher, J., Aziz, M. J., Karma, A., Dimitrov, N. & Sieradzki, K. Evolution of nanoporosity in dealloying. *Nature* **410**, 450–453 (2001).
24. Schofield, E. J., Ingham, B., Turnbull, A., Toney, M. F. & Ryan, M. P. Strain development in nanoporous metallic foils formed by dealloying. *Appl. Phys. Lett.* **92**, 1–4 (2008).
25. Simoes, T. A. et al. Microstructural characterization of low and high carbon CoCrMo alloy nanoparticles produced by mechanical milling. *J. Phys. Conf. Ser.* **522**, 12059 (2014).
26. Kerker, M., Robinson, J. & Forty, A. J. In situ structural studies of the passive film on iron and iron/chromium alloys using X-ray absorption spectroscopy. *Faraday Discuss. Chem. Soc.* **89**, 31–40 (1990).
27. Tay, S. E. R. et al. Direct in situ observation of ZnO nucleation and growth via transmission X-ray microscopy. *Nanoscale* **8**, 1849–1853 (2016).



**Open Access** This article is licensed under a Creative Commons Attribution 4.0 International License, which permits use, sharing, adaptation, distribution and reproduction in any medium or format, as long as you give appropriate credit to the original author(s) and the source, provide a link to the Creative Commons license, and indicate if changes were made. The images or other third party material in this article are included in the article's Creative Commons license, unless indicated otherwise in a credit line to the material. If material is not included in the article's Creative Commons license and your intended use is not permitted by statutory regulation or exceeds the permitted use, you will need to obtain permission directly from the copyright holder. To view a copy of this license, visit <http://creativecommons.org/licenses/by/4.0/>.

© The Author(s) 2018